Mehdizadeh, F., Barzegar-Jalali, M., Izadi, E., Osouli Bostanabad, K., Mohaghegh, S., Shakeri, M. S., Nazemiyeh, H., & Omidi, Y. (2022).
Green and chemical reduction approaches for facile pH-dependent synthesis of gold nanoparticles.
Inorganic and Nano-Metal Chemistry, 1-9.
https://doi.org/10.1080/24701556.2022.2078357

Green and chemical reduction approaches for facile pH-dependent synthesis of gold nanoparticles

Fatemeh Mehdizadeh[a,b], Mohammad Barzegar-Jalali[c], Ebrahim Izadi[d], Karim Osouli-Bostanabad[a,b], Seraj Mohaghegh[a,b], Mohammad Sadegh Shakeri[e] , Hossein Nazemiyeh[a], Yadollah Omidi[f], and Khosro Adibkia[a]

[a] Research Center for Pharmaceutical Nanotechnology, and Faculty of Pharmacy, Tabriz University of Medical Sciences, Tabriz, Iran;

[b] Students Research Committee, Tabriz University of Medical Sciences, Tabriz, Iran;

[c] Pharmaceutical Analysis Research Center, Tabriz University of Medical Sciences, Tabriz, Iran;

[d] Department of Materials Engineering, Faculty of Mechanical Engineering, University of Tabriz, Iran;

[e] Materials and Energy Research Center (MERC), Meshkindasht, Karaj, Iran;

[f] Department of Pharmaceutical Sciences, College of Pharmacy, Nova Southeastern University, Fort Lauderdale, FL, USA

Correspondence: Khosro Adibkia adibkia@tbzmed.ac.ir Research Center for Pharmaceutical Nanotechnology, and Faculty of Pharmacy, Tabriz University of Medical Sciences, Tabriz, Iran.

Abstract

This study compares the green synthesis method using the Lycium ruthenicum (*L. Ru*) with wet chemical extraction using citrate reduction to synthesize stable gold nanoparticles (AuNPs). The effect of pH on the synthesized AuNPs has also been evaluated in the present investigation. AuNPs were synthesized successfully by both methods, as well; by the way, there were reported differences between the microstructure of resulting powders. For AuNPs synthesized using the green method, a pH value of 3 was reported to be the optimum pH due to the characteristics of synthesized AuNPs. In the mentioned pH, the AuNPs were spherical, mono-dispersed, and highly crystalline, characteristic of a well-done synthesis. Both chemo- and biosynthesized AuNPs revealed a relatively smaller particle size (33.92 and 55.65 nm, respectively) with well-dispersed spherical morphology under alkaline conditions. This study revealed that employing *L. Ru* extract could be considered a simple, facile, and green technique in stimuli-sensitive AuNPs synthesis.

Introduction

By the progression of nanotechnology, the synthesis of noble metal nanoparticles has always been one of the critical fields that attracted the attention of scientists in this field. Gold is one of these noble metals and its nanoparticles (AuNPs) synthesis has received enormous attention during the last two decades due to its fascinating applications. Distinctive electrical, optical, and photothermal characteristics of AuNPs have enabled its applications in biochemical/chemical sensing, catalysis, photonics, cosmetics, pharmaceuticals, biotechnology, and so on. [1–3] Morphology, size, and surface characteristics play vital roles in controlling the aforementioned unique properties of AuNPs. For instance, it has been shown that the cytotoxicity of AuNPs depends on their size in medicine and biology.[4] It has also been demonstrated that the catalytic performance in chemical catalysis, optical properties, and the AuNPs plasmon absorption characteristics are the morphology and size dependent. [5,6] The preparation of AuNPs with controlled morphology and size potentially applicable in cosmetics and biomedicine has turned to be the focal point of various research works. Therefore, several feasible methods have recently been employed for the synthesis of AuNPs, including photochemical,[7,8] radiolytic, [9] sonochemical,[10] and chemical reduction. [1] Among these techniques, wet chemistry (i.e., chemical reduction in a solution) benefiting sodium borohydride or citrate as a reducing agent was determined as the most popular

procedure for preparing AuNPs. However, the drawbacks of these methods were their high process costs besides using toxic compounds and organic solvents. The disadvantages of the mentioned methods paved the way for establishing an economically sound green nanotechnology using biological materials such as bacteria, fungi, viruses, algae, and plants. [11–14]

Different kinds of plants, including Azadirachta Indica,[15] Cinnamomum Camphora,[16] Eucommia Ulmoides,[17] Aloe Vera,[18] Gymnema Sylvestre,[19] and Hibiscus Sabdariffa[20] have been benefited to synthesize stable bioactive and biocompatible AuNPs with prospective usages in the medical realm.[21,22] Biomolecules present in plant extracts (i.e., terpenoids, phenolic compounds, alkaloids, and co-enzymes) can be employed as the reducing agents for production of metal NPs in a one-step green synthesis procedure. The base metal formation from its metal ions using these biogenic water-soluble reducing biomolecules is relatively quick, effortlessly conducted at ambient pressure that can be simply scaled up. These extracts may behave as both stabilizing and reducing agents in the NPs synthesis process. It has also been evidenced that the plant extraction could affect the characteristics of synthesized NPs.[23] This is due to the fact that various extract agents contain diverse combinations and concentrations of the reducing agents.[24]

There are numerous studies on berries and dried Lycium fruits (goji berries, wolfberries, Fructus lycii) that are utilized in some researches. [25,26] There are around eighty types of Solanaceae (Lycium L) globally, [26,27] but just three forms (L. chinense, L. barbarum, L. ruthenicum) are employed as a medicine, including siyah goji or goji berries. Lycium ruthenicum (L. Ru), an endangered wild everlasting thorny shrub, exists in the Mediterranean and across Asia. Modern pharmacological studies have proved that L. Ru has numerous pharmaceutical influences, including anti-aging, antioxidant,[28] immune-enhancement,[29] anti-fatigue, [30] and radio-resistance effects. The compounds in L. Ru include anthocyanins, flavonoids, phenolic acids, polysaccharides, carotenoids, essential oils, alkaloids, and fatty acids.[31,32]

By a comprehensive literature review, it has been found out that L. Ru extract has not been employed as a reducing and capping agent for synthesizing of AuNPs. The main focus of the current work is on the synthesis of AuNPs using the L. Ru extract and controlling the size and morph- ology of nanoparticles using pH. Accordingly at the first step, it has been tried to synthesize AuNPs using L. Ru and sodium citrate reducing agents at various pH values. This investigation

proceeds with the comparison of two synthesizing methods, evaluation of physicochemical behavior of synthesized samples, and evaluation of the role of synthesizing mechanism on morphology and size of the synthesized AuNPs.

Methods and materials

Materials

In the current study, the entire chemical substances and solvents were supplied by Sigma Aldrich and employed without any purification. In addition, Milli-Q water (ultra-pure) with specific resistivity equals to 18.2 MX cm was employed in all experiments as a solvent.

Preparation of Lycium ruthenicum extract

The plant fruit was harvested in University of Tabriz Campus, Tabriz, Iran. L. Ru identification was conducted at the herbarium of Tabriz University of Medical Sciences [TbzMed herbarium sample number: 4039 (tbz-fph)]. A sufficient amount of L. Ru fruits were washed using distilled water for removing any dust and impurity. Approximately, 600 g of L. Ru fresh fruits was squeezed and submerged in 70% ethanol with a 1:3 wt/vol ratio of L. Ru:ethanol at room temperature for 72 h while shaking at 300 rpm. The produced extract was then filtered using the Whatman filter paper No. 1. Afterward, a rotary evaporator (Heidolph Persia, Tehran, Iran) in rotating speed of 100 rpm was employed at 40 ^{0}C under reduced pressure (low pressure) to condense the filtered extract by eliminating the ethanol Ultimately, the crude extract in a dried and concentrated state was weighed accurately and stored at 4 ^{0}C.

Green synthesis method

Before the addition of L. Ru extract (5% wt/vol), 10 mL of 1 mM HAuCl 4 solution (pH ¼ 3) was heated to reach the temperature of 85 ^{0}C. Moreover, to uphold the pH of a HAuCl 4 solution at the desired value, sodium hydroxide 0.1 N was utilized. Three samples were prepared with pH of 3, 7, and 8.5. Following the pH adjustment, L. Ru extract was drop-wisely added (1 mL) to the HAuCl4 solution and left for 20 min under continuous agitation to reduce Au ions to Au 0 . The generation of Au0 particles was indicated by the solution color change from yellowish solution to wine red. Eventually, the final suspension was centrifuged for 15 min at 13,000 rpm for three times.

The wet chemical synthesis method

Concerning the chemical method of AuNPs synthesis com- pared to the biosynthesis method, sodium citrate was used as the reducing agent in the wet chemical technique. A 1% wt/vol solution of sodium citrate was made by dissolving tri-sodium citrate (1 g) in 100 mL of distilled water and employed as the reducing agent. The steps of Au particles synthesis through the chemical method were the same as the green synthesis method.

Characterization

UV–visible study

The ultraviolet–visible spectrophotometry (UV–visible, Shimadzu, Japan) was performed to visualize the presence of excitation spectra (surface plasmon resonance) of synthesized colloidal solutions in the range of 400–700 nm with 60 nm/min scan rate.

Fourier-transform infrared spectroscopy

Green synthesized nanoparticles were analyzed by Fourier transform infrared (FTIR) spectrophotometer (Shimadzu 43000, Kyoto, Japan) for the evaluation of molecular bonding. To this end, the nanoparticles were compressed to form a disk using the KBr disk method and analyzed with 32 spectra scans in 4000–600 cm^{-1} scan range at a resolution of 2 cm^{-1} .

Powder X-ray diffraction and X-ray energy dispersive analyses

A powder X-ray diffractometer (Siemens D 5000, Germany) with 0.6 ^{0}/min scanning rate was used to assess the patterns of the synthesized samples in a 2ɵ angle range of 10–85 at a step size 0.02^{0}. The working variables were the copper K(alpha) radiation (wavelength = 1.5405 Å) at 30 mA, 40 kV. The elemental constitution of particles was measured by a field-emission scanning electron microscope (MIRA3_FE-SEM, Tescan Co., Czech) equipped with the X-ray energy dispersive (EDX) detector.

Figure 1

Transmission electron microscopy, FE-SEM, and dynamic light scattering evaluations

The FE-SEM and a transmission electron microscope (TEM) (Tecnai, 20 G2) operating at 20 kV and 80 kV, respectively, were used to determine the shape and size of the prepared samples. Gold

sputtering machine (K550_Emitech, UK) was utilized to coat the synthesized samples with a thin gold layer before FE-SEM assessments. Finally, a dynamic light scattering (DLS) device (Microtrac, Nanotrac Wave, USA) was used to evaluate the average particle size as well as the index of polydispersity (PDI) of the prepared samples.

Results and discussion

UV–visible spectrophotometry

Once the metal NPs are excited by a particular wavelength of light, they would present a distinctive surface phenomenon known as surface plasmon resonance (SPR). Oscillation of the conduction band electrons on the metal NPs surface combined with the light wave is the cause of the observation of the SPR absorption band. SPR phenomenon may individually establish a distinct peak for each type of metal NPs using UV–vis technique. At the moment after mixing the reducing agents (L. Ru extract and 1% solution of sodium citrate) with hydrogen tetrachloroaurate solution (pale yellow), a noticeable color change was observed (it turned to wine red) (Figure 1). This color change visually confirmed the formation of AuNPs, where a transition in color could be commonly considered an indicator of alterations in the oxidation state of the metal. The SPR excitation of the synthesized AuNPs was the reason for this color change, as declared in other studies. [33,34] The nanoparticle of metals with different sizes and morphologies displays various colors when used in different solutions; consequently, morphologies of the synthesized particles can be visually evaluated based on the variations in the color of solutions. For instance, a black or blue, purple or wine red, and golden yellow colors of the solution represent the Au nanorods, spherical AuNPs, and metallic Au formation, respectively. [35,36] The UV–vis absorption spectra of suspended AuNPs adding L. Ru (5% wt/vol) extract and sodium citrate (1% wt/vol) solution to 1 mM solution of HAuCl 4 with different values of pH at 85 ^{0}C after 20 minutes are shown in Figure 2.

Figure 2

Spectral evaluation of the samples reduced using the L.Ru extract indicates that the UV SPR peak at 520 nm has been generally considered for AuNPs. The SPR peak as mentioned earlier was enhanced intensely as the pH values were decreased from 8.5 to 3 with a redshift in the peak position (532 nm at pH 3) (Figure 2b). Here, the effect of adding 1% sodium citrate solution as a chemical reducing agent was also examined on AuNPs synthesis. Figure 2 indicates that the SPR

peak intensity of these specimens in the UV–vis absorption spectral is increased clearly with a reduction in the pH value from 8.5 to 3 with a slight shift in the peak position. In the present study, Au0 was formed by reduction of Au^{3+} ions benefiting L. Ru extract biomolecules that will be evaluated using FTIR assessments. Studies on various metal NPs have proposed that their SPR frequencies strictly depend on their morphologies, sizes, and agglomeration states. [33,34,37] AuNPs with spherical morphology with a diameter of about 30 nm exhibit a strong SPR absorption peak at around 520 nm. An increase in the diameter of the synthesized NPs would result in a redshift to longer wavelengths for this band [38]; contrariwise, a decrease in the diameter of these particles would lead to the blueshift of this band to the lower wavelength (Figure 2b). The blueshift of the SPR band and the augmentation of oscillator strength indicate the reduction in the size of particles due to quantum confinement effects. [39] UV–vis data (Figure 2) implied that the synthesized AuNPs under various pH values were nanosized and had spherical and semi-spherical morphologies which will be discussed more by TEM, FE-SEM, and DLS results.

Furthermore, according to Figure 2, the reduction of pH values from 8.5 to 3 increased the intensity of the SPR band of AuNPs, illustrating that a large amount of AuNPs could be synthesized at a low pH of the reaction medium. This result might be clarified because at a lower pH, the carboxylate (COO-) groups of L. Ru could reduce the Au^{3+} ions more efficiently than at a higher pH, resulting in the augmentation of AuNPs in the aqueous solution (Figure 3). The same trend was detected in the samples reduced by citrate solution; however, instead of a redshift occurred in the biosynthesized AuNPs, a blueshift was observed in these samples. In other words, the SPR band positions were slightly changed from 520 nm at pH 8.5 to 514.5 nm at pH 3 (Figure 2b). In addition, Figure 2a indicates that the SPR band of the biosynthesized AuNPs became narrower and sharper as the pH decreased from 8.5 to 3. The same phenomena happened to the chemo-synthesized AuNPs (i.e., a narrow and intense SPR band was achieved when the pH decreased from 8.5 to 3), demonstrating a more limited dispersion and higher yield of AuNPs. The different trends of the absorption wavelength change in green and wet chemical methods are attributed to the molecular surface group, which is altered by pH, and the reducing agent, which is entirely in agreement with the previously published research.[37–3]

Figure 3

FTIR data analysis

The FTIR spectrum can be employed as a fingerprint for recognizing different molecules by comparing the spectrum of an unknown sample with that of the formerly recorded reference sample. In addition, FTIR evaluation can be employed to recognize functional groups in a sample. Hence, the FTIR test was carried out in the current study to detect the possibly involved functional groups of the L. Ru extract in the reduction and capping of Au ions into their corresponding NPs. Figure 3 indicates the FTIR spectrum of the L. Ru extract and the samples synthesized at 85 ^{0}C using extract solution (5% wt/vol) in pH values of 3, 7, and 8.5 after 20 min. The spectral profile of the native L. Ru extract displayed several functional groups, among which 3409, 2928, 2357, 1629, 1412, and 1061 cm^{-1} bands were more dominant. The aforementioned spectral bands could be associated with the -OH stretching vibration of the functional groups within phenolic compounds, alkane groups -CH stretching vibrations, stretching vibrations of asymmetrical and symmetrical COO-, as well as the C-O-H stretching vibration.[33,37]

Figure 4

Considering the FTIR peaks of the treated specimens, biosynthesized samples had the polyphenolic –OH, alkanes groups -CH stretching vibrations, and the stretching carboxylic acid group. These findings implied that biomolecules in L. Ru extract could be predominantly involved in reducing Au ions into AuNPs. Similar results have been published for bio-fabrication of Ag ions, declaring the involvement of these functional groups in Sargassum polycystum aqueous extract. [40] The small band shifts might be associated with the interaction of Au ions with the functional groups of L. Ru extract. The proposed mechanism for forming gold nanoparticles using the green synthesizing method has been quoted to be the reduction process of extraction using flavonoids, antioxidant, and phenolic molecules. These molecules donate hydrogen atoms or electrons. Hence, Au nanoparticles are decreased from HAuCl 4 and act as Au 0 seeds, nucleation sites for further reducing Au nanoparticles. [41]

The mechanism for reducing Au ions to Au 0 in the chemosynthesis process is proposed to be the formation of sodium acetone dicarboxylate (due to citrate oxidation) following the blending of citrate 1% at a high temperature with the hydrogen tetrachloroaurate solution (HAuCl4) in the water, where AuCl would form due to the reduction of HAuCl 4. Simultaneously, on the basis of pH values of the reaction solution, the Au ($AuCl^{+4}$) ions are hydrolyzed to various kinds of auric (Au) precursor ions, including Au(OH)4 , AuCl(OH)3 , AuCl 2(OH) 2 , and AuCl 3(OH)

corresponding to pH values of 12.9, 8.1, 7.1, and 6.2, respectively. Subsequently, the reactive function of the Au precursor ions have a decreasing trend, where the highest reactivity corresponds to AuCl 4–, the lowest reactivity assigns to Au(OH)4–, AuCl3 (OH)– has a higher reactivity compared to AuCl2 (OH) 2– (but less than AuCl 4–), and AuCl(OH) 3– has a higher reactivity compared to Au(OH) 4– (but less than AuCl2 (OH) 2–).[42–44]

PXRD and EDX assessments

The powder X-ray diffraction (PXRD) analysis was conducted to scrutinize the crystalline structure, as well as the phase structure of prepared AuNPs. Figure 4a demonstrates the PXRD peaks of AuNPs synthesized using L. Ru extract and citrate 1% solution at pH values of 3, 7, and 8.5. The peaks at these patterns (Figure 4a) could imply the cubic structure of the Au phase with a lattice constant of 4.0699 Å (JCPDS No. 004-0784 and No. 001-1172). Lack of any diffraction peaks other than those from as-synthesized samples proposed high purity of the Au phase. In addition, the sharp and strong peaks revealed well crystallization of as-synthesized gold particles. The five typical peaks at 2h angles, namely, 38.27, 44.6, 64.68, 77.55, and 82.35 might be associated with the diffraction from the (111), (200), (220), (311), and (222) planes, respectively, resulted from the face-centered cubic (FCC) crystalline structure of Au. As it is clear in Figure 4, the corresponding peak to the plane (111) was narrower and more intense than the other Bragg reflection peaks from the planes (200), (220), and (311), implying that the synthesized Au nanocrystals were preferably oriented along this plane. Widening the peaks might be due to the crystallite size or diffracting domain alterations, structural defects (i.e., twin and/or stacking faults), crystal lattice distortion (micro-strain produced due to dislocations or concentration gradients), and so on. Considering Figure 4a, it is clear that the PXRD peaks became broader with increasing pH values, suggesting the formation of AuNPs with a smaller size. [21,33,38] On the other hand, the peaks for AuNPs synthesized in higher pH have a lower level of crystallinity which is completely obvious from the sharper peaks accompanied with the sample synthesized in pH value equal to 3.

Figure 5

Figure 4b depicts the characteristic EDX spectrum of AuNPs synthesized using L. Ru extract at pH 3 with its percentage of elements weight. A strong, distinctive peak detected at around 2.0 keV is the unique absorption peak of the Au match with AuNPs SPR. Moreover, some peaks of Na, C,

and O were also identified, possibly resulted from the involvement of L. Ru extract in the formation of AuNPs.

Figure 6

PXRD and EDX results were in line with those of UV–vis (Figure 2) and also corresponds to previously published articles.[21,33,37,38]

Analysis of morphological and particle size distributions

FE-SEM, TEM, and DLS tests were performed to acquire a straight insight into the AuNPs particle size and their distributions [i.e., the morphology, particle size, and polydispersity index (PDI) of the resultant samples]. Figures 5 and 6 show the FE-SEM and DLS data of AuNPs prepared using bio- and chemo-synthesis processes, respectively. The UV–vis spectra (Figure 2) and PXRD data (Figure 4) associated with the effect of pH of the L. Ru extract on the particle size of the as-synthesized AuNPs were precisely corroborated by FE-SEM and DLS observations.

Figure 7

FE-SEM results revealed that the greenly synthesized AuNPs in all pH values were mainly spherical and semi- spherical (Figure 5a–c). Moreover, DLS results demonstrated that the average particle sizes of NPs were about 188.50, 81.82, and 55.65 nm, corresponded to pH values of 3 (Figure 5a), 7 (Figure 5b), and 8.5 (Figure 5c), respectively. As the pH value of L. Ru extract decreased from 8.5 to 3, the synthesized AuNPs seemed to develop almost spherical morphology with an escalation in the particle size. The PDIs of the biosynthesized AuNPs were found to be 0.316 (pH 3), 0.525 (pH 7), and 0.863 (pH 8.5) (Figure 5a0–c0). According to the literature, the pH adjustment in reducing a solution could affect the shape, as well as the size of the synthesized AuNPs. [37,38]

The chemo-synthesized AuNPs (Figure 6) revealed spherical morphology with the average particle sizes of 37.21, 33.15, and 33.92 nm at pH values of 3 (Figure 6a), 7 (Figure 6b), and 8.5 (Figure 6c), respectively. The PDIs of these samples were found to be 0.76, 0.517, and 0.468 at pH values of 3, 7, and 8.5, respectively (Figure 6a0–c0).

TEM assessments (Figure 7) revealed that the as-synthesized AuNPs using L. Ru extract at pH 8.5 were pretty spherical with an almost smooth surface. In comparison, the

as-synthesized AuNPs using citrate 1% showed semi-spherical shapes with almost well-distributed particle sizes.

Conclusion

In summary, it was tried to synthesize AuNPs using reduction of HAuCl 4 by L. Ru extract as a green synthesis and citrate solution as a wet chemical method. The pH of the HAuCl 4 solution was changed in values of 3, 7, and 8.5 for both synthesizing methods. The results show that both methods are capable of high-efficiency production of AuNPs, as well; by the way, there are differences between resulted powder microstructures due to different mechanisms of reduction. For AuNPs synthesized using the green energy method, a pH value of 3 is the optimum pH among the analyzed pH values due to the extraction of spherical, mono-dispersed, highly crystallized particles with higher production efficiency related to other samples. However, AuNPs synthesized at a pH value of 3 have a bigger size which could be attributed to higher tendency of them for crystallization.

Author contributions

FM did the experiments and collected the data. YO and MBJ contributed to the study consultation, conceptualization of the manuscript, and to the overall writing and editing of the manuscript. EI and SM analyzed the data, presented data. HN and MSS contributed to data analysis and data presentation. KOB and KA conceived the original idea, supervised the project, designed the experiments, aided in interpretation of data, contributed to data analysis, data presentation, and writing and reviewing of the manuscript. All authors discussed the contents and contributed to the final manuscript.

Funding

Elite Researcher Grant Committee supported the study under award number (No. 971027) from the National Institutes for Medical Research Development (NIMAD), Tehran, Iran.

ORCID

Yadollah Omidi http://orcid.org/0000-0003-0067-2475

Khosro Adibkia http://orcid.org/0000-0002-1053-5557

References

1. Bai, X.; Wang, Y.; Song, Z.; Feng, Y.; Chen, Y.; Zhang, D.; Feng, L. The Basic Properties of Gold Nanoparticles and Their Applications in Tumor Diagnosis and Treatment. Int. J. Mol. Sci. 2020, 21, 2480. DOI: 10.3390/ijms21072480.

2. Siddique, S.; Chow, J. C. Gold Nanoparticles for Drug Delivery and Cancer Therapy. Appl. Sci. 2020, 10, 3824. DOI: 10.3390/ app10113824.

3. Molnar, Z.; Bodai, V.; Szakacs, G.; Erdelyi, B.; Fogarassy, Z.; Safrn, G.; Varga, T.; Knya, Z.; Toth-Szeles, E.; Szucs, R.; Lagzi, I. Green Synthesis of Gold Nanoparticles by Thermophilic Filamentous Fungi. Sci. Rep. 2018, 8, 3943. DOI: 10.1038/ s41598-018-22112-3.

4. Chen, Y.; Yang, J.; Fu, S.; Wu, J. Gold Nanoparticles as Radiosensitizers in Cancer Radiotherapy. Int. J. Nanomed.. 2020, 15, 9407–9430. DOI: 10.2147/IJN.S272902.

5. Narayanan, R.; El-Sayed, M. A. Shape-Dependent Catalytic Activity of Platinum Nanoparticles in Colloidal Solution. Nano Lett. 2004, 4, 1343–1348. DOI: 10.1021/nl0495256.

6. Moore, J. A.; Chow, J. C. Recent Progress and Applications of Gold Nanotechnology in Medical Biophysics Using Artificial Intelligence and Mathematical Modeling. Nano Express 2021, 2, 022001. https://orcid.org/0000-0003-4202-4855. DOI: 10.1088/ 2632-959X/abddd3.

7. Chevychelova, T. A.; Zvyagin, A. I.; Perepelitsa, A. S.; Ovchinnikov, O. V.; Smirnov, M. S.; Selyukov, A. S. Role of Photoinduced Destruction of Gold Nanorods in the Formation of Nonlinear Optical Response. Optik 2022, 250, 168352. DOI: 0.1016/j.ijleo.2021.168352.

8. Xiang, Q.; Wu, Z.; Tian, E. K.; Nong, S.; Liao, W.; Zheng, W. Gold Nanoparticle Drug Delivery System: Principle and Application. J. Biomater. Tissue Eng. 2022, 12, 445–460. DOI: 10. 1166/jbt.2022.2934.

9. Tue Anh, N.; Van Phu, D.; Ngoc Duy, N.; Duy Du, B.; Quoc Hien, N. Synthesis of Alginate Stabilized Gold Nanoparticles by c-Irradiation with Controllable Size Using Different Au^{3+} Concentration and Seed Particles Enlargement. Radiat. Phys. Chem. 2010, 79, 405–408. DOI: 10.1016/j.radphyschem.2009.11.013.

10. Okitsu, K.; Mizukoshi, Y.; Yamamoto, T. A.; Maeda, Y.; Nagata, Y. Sonochemical Synthesis

of Gold Nanoparticles on Chitosan. Mater. Lett. 2007, 61, 3429–3431. DOI: 10.1016/j.matlet.2006.11.090.

11. Pandey, S.; Nanda, K. K. Au Nanocomposite Based Chemiresistive Ammonia Sensor for Health Monitoring. ACS Sens. 2016, 1, 55–62. DOI: 10.1021/acssensors.5b00013.

12. Thakkar, K. N.; Mhatre, S. S.; Parikh, R. Y. Biological Synthesis of Metallic Nanoparticles. Nanomedicine 2010, 6, 257–262. DOI:10.1016/j.nano.2009.07.002.

13. Gholami-Shabani, M.; Shams-Ghahfarokhi, M.; Gholami-Shabani, Z.; Akbarzadeh, A.; Riazi, G.; Ajdari, S.; Amani, A.;Razzaghi-Abyaneh, M. Enzymatic Synthesis of Gold Nanoparticles Using Sulfite Reductase Purified from Escherichiacoli: A Green Eco-Friendly Approach. Process Biochem. 2015, 50,1076–1085. DOI: 10.1016/j.procbio.2015.04.004.

14. Mohaghegh, S.; Osouli-Bostanabad, K.; Nazemiyeh, H.;Javadzadeh, Y.; Parvizpur, A.; Barzegar-Jalali, M.; Adibkia, K. A Comparative Study of Eco-Friendly Silver Nanoparticles Synthesis Using Prunus Domestica Plum Extract and Sodium Citrate as Reducing Agents. Adv. Powder Technol. 2020, 31,1169–1180. DOI: 10.1016/j.apt.2019.12.039.

15. Shankar, S. S.; Rai, A.; Ahmad, A.; Sastry, M. Rapid Synthesis of Au, Ag, and Bimetallic Au core-Ag shell nanoparticles using Neem (Azadirachta indica) leaf broth. J. Colloid Interface Sci. 2004, 275, 496–502. DOI: 10.1016/j.jcis.2004.03.003.

16. Narayanan, K. B.; Sakthivel, N. Coriander Leaf Mediated Biosynthesis of Gold Nanoparticles. Mater. Lett. 2008, 62, 4588–4590. DOI: 10.1016/j.matlet.2008.08.044.

17. Guo, M.; Li, W.; Yang, F.; Liu, H. Controllable Biosynthesis of Gold Nanoparticles from a Eucommia Ulmoides Bark Aqueous Extract. Spectrochim. Acta A Mol. Biomol. Spectrosc. 2015, 142, 73–79. DOI: 10.1016/j.saa.2015.01.109.

18. Chandran, S. P.; Chaudhary, M.; Pasricha, R.; Ahmad, A.; Sastry, M. Synthesis of Gold Nanotriangles and Silver Nanoparticles Using Aloe vera plant extract. Biotechnol. Prog. 2006, 22,

577–583. DOI: 10.1021/bp0501423.

19. Nakkala, J. R.; Mata, R.; Bhagat, E.; Sadras, S. R. Green Synthesis of Silver and Gold Nanoparticles from Gymnema Sylvestre Leaf Extract: study of Antioxidant and Anticancer

Activities. J. Nanopart. Res. 2015, 17, 151. DOI: 10.1007/s11051-015-2957-x.

20. Mishra, P.; Ray, S.; Sinha, S.; Das, B.; Khan, M. I.; Behera, S. K.; Yun, S.-I.; Tripathy, S. K.; Mishra, A. Facile Bio-Synthesis of Gold Nanoparticles by Using Extract of Hibiscus Sabdariffa and Evaluation of Its Cytotoxicity against U87 Glioblastoma Cells under Hyperglycemic Condition. Biochem. Eng. J. 2016, 105, 264–272. DOI: 10.1016/j.bej.2015.09.021.

21. Miri, A.; Darroudi, M.; Entezari, R.; Sarani, M. Biosynthesis of Gold Nanoparticles Using Prosopis Farcta Extract and Its in Vitro Toxicity on Colon Cancer Cells. Res. Chem. Intermed. 2018, 44, 3169–3177. DOI: 10.1007/s11164-018-3299-y.

22. Majdi, H.; Salehi, R.; Pourhassan-Moghaddam, M.; Mahmoodi, S.; Poursalehi, Z.; Vasilescu, S. Antibody Conjugated Green Synthesized Chitosan-Gold Nanoparticles for Optical Biosensing. Colloid Interface Sci. Commun. 2019, 33, 100207. DOI: 10.1016/j. colcom.2019.100207.

23. Kumar, V.; Yadav, S. K. Plant-Mediated Synthesis of Silver and Gold Nanoparticles and Their Applications. J. Chem. Technol. Biotechnol. 2009, 84, 151–157. DOI: 10.1002/jctb.2023.

24. Mukunthan, K. S.; Balaji, S. Cashew Apple Juice (Anacardium occidentale L.) Speeds up the Synthesis of Silver Nanoparticles. Int. J. Green Nanotechnol. 2012, 4, 71–79. DOI: 10.1080/ 19430892.2012.676900.

25. Seeram, N. P. Berry Fruits: Compositional Elements, Biochemical Activities, and the Impact of Their Intake on Human Health, Performance, and Disease. J. Agric. Food Chem. 2008, 56, 627–629. DOI: 10.1021/jf071988k.

26. Miller, J. S: Phylogenetic Relationships and the Evolution of Gender Dimorphism in Lycium (Solanaceae). Systematic Botany 2002, 27, 416–428.

27. Levin, R. A.; Miller, J. S. Relationships within Tribe Lycieae (Solanaceae): Paraphyly of Lycium and Multiple Origins of Gender Dimorphism. Am. J. Bot. 2005, 92, 2044–2053. DOI: 10.

3732/ajb.92.12.2044.

28. Hu, N.; Zheng, J.; Li, W.; Suo, Y. Isolation, Stability, and Antioxidant Activity of Anthocyanins from Lycium Ruthenicum Murray and Nitraria Tangutorum Bobr of Qinghai-Tibetan Plateau. Sep. Sci. Technol. 2014, 49, 2897–2906. DOI: 10.1080/

01496395.2014.943770.

29. Gong, Y.; Wu, J.; Li, S.-T. Immuno-Enhancement Effects of Lycium Ruthenicum Murr. polysaccharide on Cyclophosphamide-Induced Immunosuppression in Mice. Int. J. Clin. Exp. Med. 2015, 8, 20631–20637.

30. Ni, W.; Gao, T.; Wang, H.; Du, Y.; Li, J.; Li, C.; Wei, L.; Bi, H. Anti-Fatigue Activity of Polysaccharides from the Fruits of Four Tibetan Plateau Indigenous Medicinal Plants. J. Ethnopharmacol. 2013, 150, 529–535. DOI: 10.1016/j.jep.2013.08.055.

31. Wang, H.; Li, J.; Tao, W.; Zhang, X.; Gao, X.; Yong, J.; Zhao, J.; Zhang, L.; Li, Y.; Duan, J-a. Lycium Ruthenicum Studies: Molecular Biology, Phytochemistry and Pharmacology. Food Chem. 2018, 240, 759–766. DOI: 10.1016/j.foodchem.2017.08.026.

32. Park, J.; Cha, S.-H.; Cho, S.; Park, Y. Green Synthesis of Gold and Silver Nanoparticles Using Gallic Acid: catalytic Activity and Conversion Yield toward the 4-Nitrophenol Reduction Reaction. J. Nanopart. Res. 2016, 18, 166. DOI: 10.1007/s11051-016-3466-2.

33. Zada, S.; Ahmad, A.; Khan, S.; Iqbal, A.; Ahmad, S.; Ali, H.; Fu, P. Biofabrication of Gold Nanoparticles by Lyptolyngbya JSC-1 Extract as Super Reducing and Stabilizing Agents: Synthesis, Characterization and Antibacterial Activity. Microb. Pathog. 2018, 114, 116–123. DOI: 10.1016/j.micpath.2017.11.038.

34. Umamaheswari, C.; Lakshmanan, A.; Nagarajan, N. S. Green Synthesis, Characterization and Catalytic Degradation Studies of Gold Nanoparticles against congo Red and Methyl Orange. J. Photochem. Photobiol. B 2018, 178, 33–39. DOI: 10.1016/j.jpho-tobiol.2017.10.017.

35. Jia, X.; Xu, X.; Zhang, L. Synthesis and Stabilization of Gold Nanoparticles Induced by Denaturation and Renaturation of Triple Helical b-Glucan in Water. Biomacromolecules 2013, 14, 1787–1794. DOI: 10.1021/bm400182q.

36. Burda, C.; Chen, X.; Narayanan, R.; El-Sayed, M. A. Chemistry and Properties of Nanocrystals of Different Shapes. Chem. Rev. 2005, 105, 1025–1102. DOI: 10.1021/cr030063a.

37. Qiu, W.-Y.; Wang, K.; Wang, Y.-Y.; Ding, Z.-C.; Wu, L.-X.; Cai, W.-D.; Yan, J.-K. pH Dependent Green Synthesis of Gold Nanoparticles by Completely C6-Carboxylated Curdlan under High Temperature and Various pH Conditions. Int. J. Biol. Macromol.

2018, 106, 498–506. DOI: 10.1016/j.ijbiomac.2017.08.029.

38. Zou, L.; Qi, W.; Huang, R.; Su, R.; Wang, M.; He, Z. Green Synthesis of a Gold Nanoparticle–Nanocluster Composite Nanostructures Using Trypsin as Linking and Reducing Agents. ACS Sustain. Chem. Eng. 2013, 1, 1398–1404. DOI: 10.1021/ sc400244u.

39. Jara, N.; Milan, N. S.; Rahman, A.; Mouheb, L.; Boffito, D. C.;Jeffryes, C.; Dahoumane, S. A. Photochemical Synthesis of Gold and Silver Nanoparticles – A Review. Molecules 2021, 26, 4585. DOI: 10.3390/molecules26154585.

40. Rajeshkumar, S.; Malarkodi, C.; Gnanajobitha, G.; Paulkumar, K.; Vanaja, M.; Kannan, C.; Annadurai, G. Seaweed-Mediated Synthesis of Gold Nanoparticles Using Turbinaria Conoides and Its Characterization. J. Nanostruct. Chem. 2013, 3, 44. DOI: 10. 1186/2193-8865-3-44.

41. Kumari, P.; Meena, A. Green Synthesis of Gold Nanoparticles from Lawsoniainermis and Its Catalytic Activities following the Langmuir-Hinshelwood Mechanism. Colloids Surf. A 2020, 606, 125447. DOI: 10.1016/j.colsurfa.2020. 125447.

42. Goia, D.; Matijevic, E. Tailoring the Particle Size of Monodispersed Colloidal Gold. Colloids Surf. A 1999, 146, 139–152. DOI: 10.1016/S0927-7757(98)00790-0.

43. Fry, F. H.; Hamilton, G. A.; Turkevich, J. The Kinetics and Mechanism of Hydrolysis of Tetrachloroaurate(III). Inorg. Chem. 1966, 5, 1943–1946. DOI: 10.1021/ic50045a024.

44. Xia, H.; Bai, S.; Hartmann, J.; Wang, D. Synthesis of Monodisperse Quasi-Spherical Gold Nanoparticles in Water via Silver(I)-Assisted Citrate Reduction. Langmuir 2010, 26, 3585–3589. DOI: 10.1021/la902987w.

Figure captions

Figure 1. The mechanism of the gold nanoparticles biosynthesis using L. Ru extract

Figure 2. (a) UV–visible spectra of AuNPs synthesized benefiting L. Ru extract (5% wt/vol) and sodium citrate (1% wt/vol) solutions at various pH states at 85 ^{0}C for 20 min; (b) The influence of pH variations on the synthesized AuNPs band wavelengths (surface plasmon resonance) employing two green and chemical reducing compounds.

Figure 3. FTIR data of L. Ru extract solutions at 85 ^{0}C and different pH values

Figure 4. (a) PXRD peaks of prepared Au nanoparticles applying citrate solution and L. Ru extract at 85 ^{0}C in different pH values; (b) representative EDX pattern of AuNPs prepared at pH 3 using solution of L. Ru extract.

Figure 5. FE-SEM images of prepared Au nanoparticles using L. Ru extract solution within controlled pH values of (a) 3, (b) 7, and (c) 8.5; (a0), (b0), and (c0) (DLS data) depict histograms of the distribution of particle sizes related to FE-SEM images of (a), (b), and (c).

Figure 6. FE-SEM images of prepared Au nanoparticles using citrate solution within controlled pH values of (a) 3, (b) 7, and (c) 8.5; (a0), (b0), and (c0) (DLS data) depict histograms of the distribution of particle sizes related to FE-SEM images of (a), (b), and (c).

Figure 7. TEM images of prepared AuNPs at 85 ^{0}C in pH 8.5 using (a) L. Ru extract solution and (b) citrate 1% solution.

Figure 1

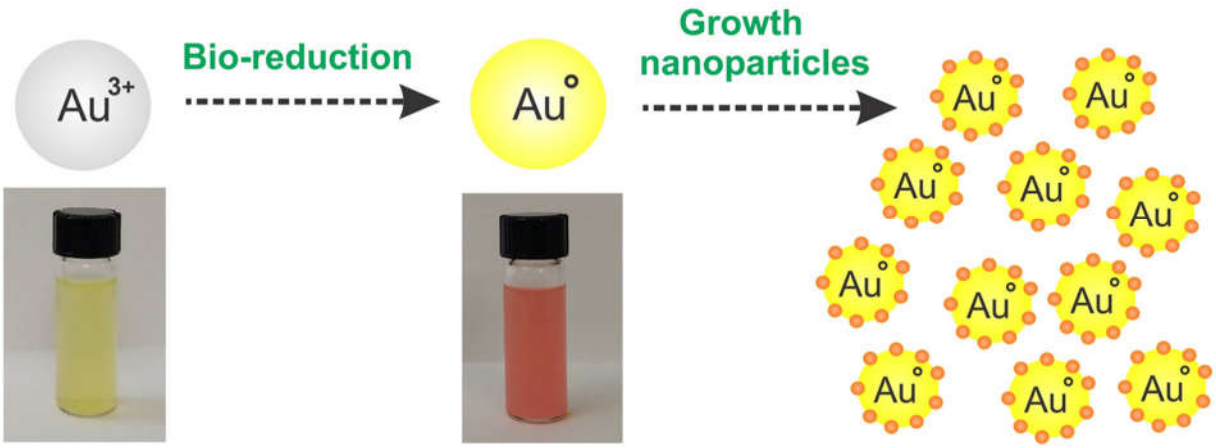

Figure 2

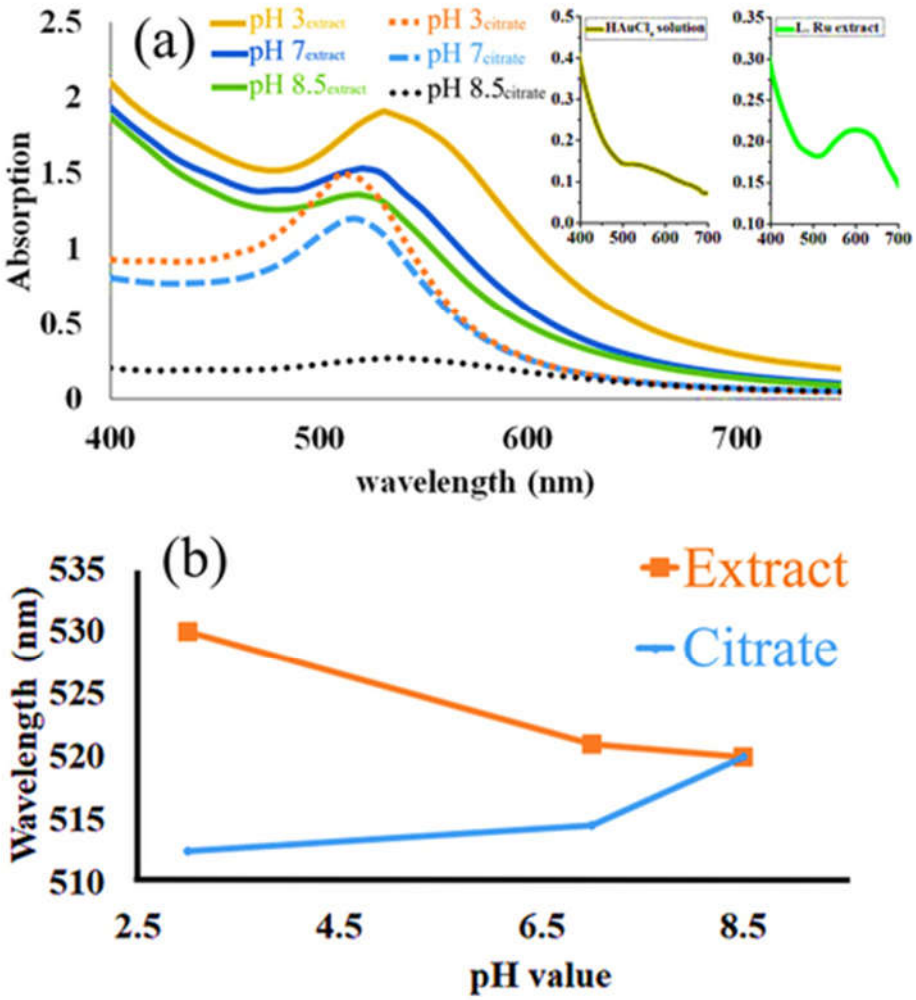
(a)
pH 3extract
pH 7extract
pH 8.5extract
pH 3citrate
pH 7citrate
pH 8.5citrate
HAuCl4 solution
L. Ru extract
Absorption
wavelength (nm)
(b)
Extract
Citrate
Wavelength (nm)
pH value

Figure 3

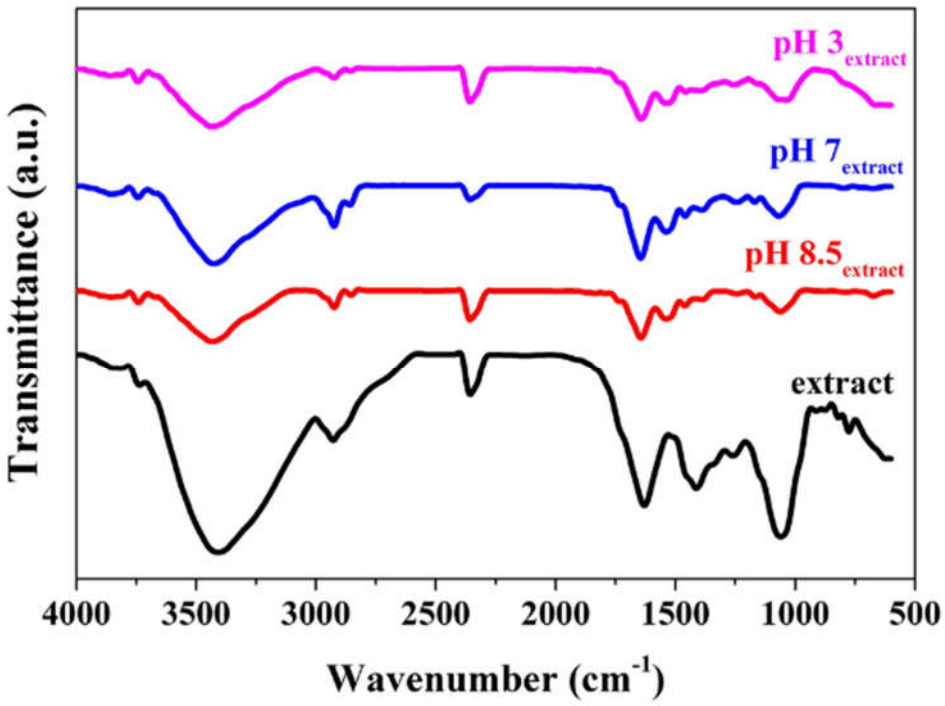
pH 3extract
pH 7extract
pH 8.5extract
extract
Transmittance (a.u.)
4000
3500
3000
2500
2000
1500
1000
500
Wavenumber (cm-1)

Figure 4

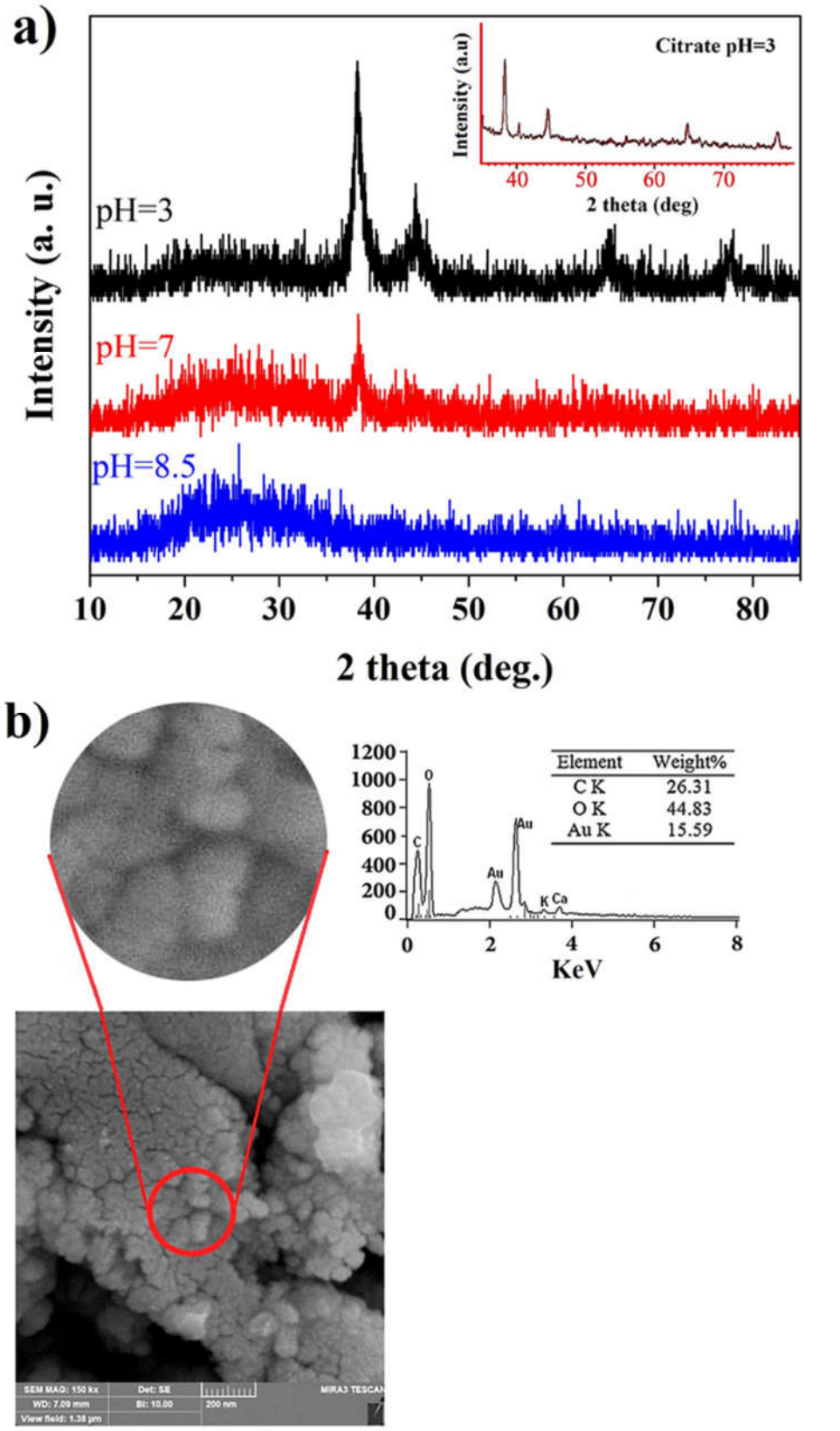
a)
Intensity (a. u.)
pH=3
pH=7
pH=8.5
10
20
30
40
50
60
70
80
2 theta (deg.)
Citrate pH=3
Intensity (a.u)
40
50
60
70
2 theta (deg)
b)
1200
1000
800
600
400
200
0
0
2
4
6
8
KeV
C
O
Au
Au
K
Ca
Element
Weight%
C K
26.31
O K
44.83
Au K
15.59
SEM MAG: 150 kx
Det: SE
MIRA3 TESCAN
WD: 7.09 mm
BI: 10.00
200 nm
View field: 1.38 µm

Figure 5

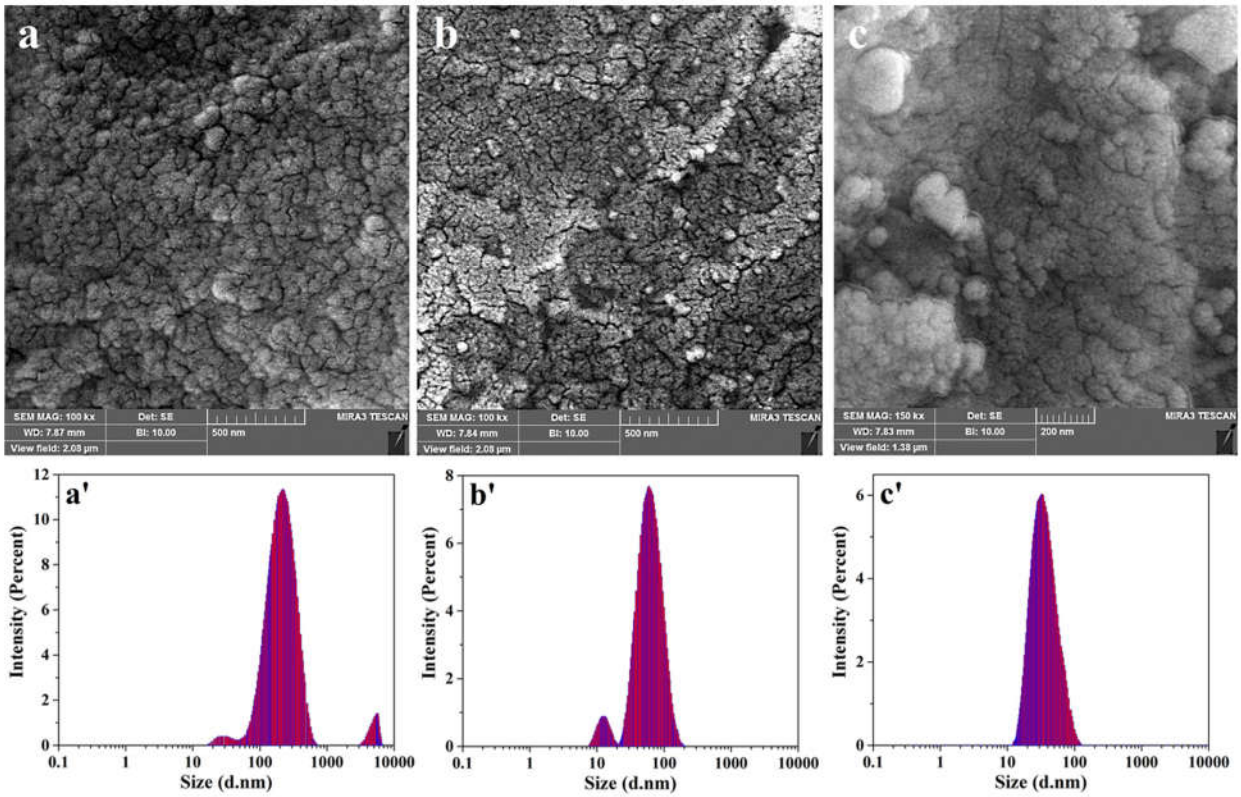
a
b
c
SEM MAG: 100 kx
Det: SE
MIRA3 TESCAN
WD: 7.87 mm
BI: 10.00
500 nm
View field: 2.08 µm
SEM MAG: 100 kx
Det: SE
MIRA3 TESCAN
WD: 7.84 mm
BI: 10.00
500 nm
View field: 2.08 µm
SEM MAG: 150 kx
Det: SE
MIRA3 TESCAN
WD: 7.83 mm
BI: 10.00
200 nm
View field: 1.38 µm
a'
b'
c'
Intensity (Percent)
Size (d.nm)
0.1
1
10
100
1000
10000

Figure 6

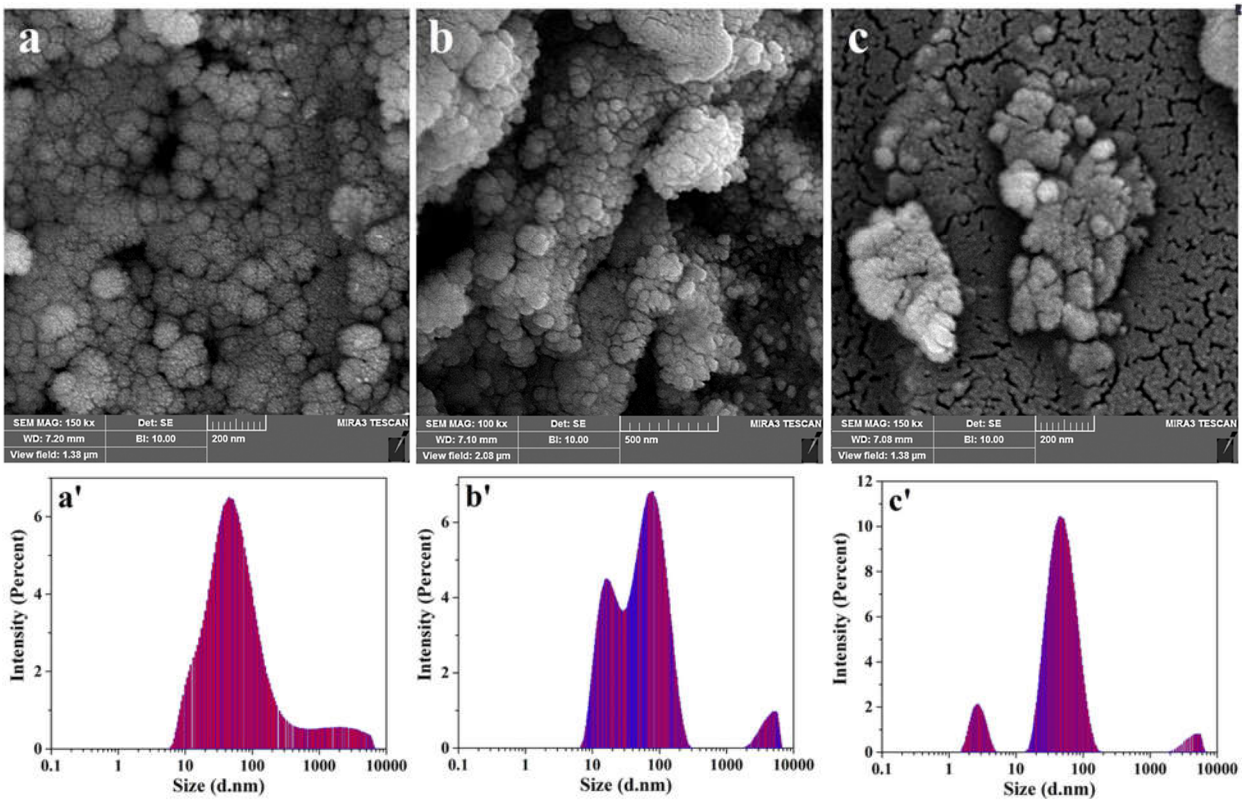
a
b
c
SEM MAG: 150 kx
Det: SE
WD: 7.20 mm
BI: 10.00
200 nm
MIRA3 TESCAN
View field: 1.38 µm
SEM MAG: 100 kx
Det: SE
WD: 7.10 mm
BI: 10.00
500 nm
MIRA3 TESCAN
View field: 2.08 µm
SEM MAG: 150 kx
Det: SE
WD: 7.08 mm
BI: 10.00
200 nm
MIRA3 TESCAN
View field: 1.38 µm
a'
b'
c'
Intensity (Percent)
Size (d.nm)
0.1
1
10
100
1000
10000

Figure 7